Materials Research Express

PAPER • **OPEN ACCESS**

Magnetisation configuration in arrays of permalloy rectangles and its impact on magnetisation reversal

To cite this article: P J Newton *et al* 2021 *Mater. Res. Express* **8** 096103

Materials Research Express

OPEN ACCESS

RECEIVED
3 August 2021

REVISED
27 August 2021

ACCEPTED FOR PUBLICATION
7 September 2021

PUBLISHED
15 September 2021

PAPER

Magnetisation configuration in arrays of permalloy rectangles and its impact on magnetisation reversal

P J Newton[1], N B Devlin[1], S M Masur[1], M Ghidini[2,3,4], D Backes[4], F Maccherozzi[4], A A Pacheco-Pumaleque[5], M A González Esqueche[6] and C H W Barnes[1]

[1] Department of Physics, Cavendish Laboratory, University of Cambridge, J. J. Thomson Avenue, Cambridge CB3 0HE, United Kingdom
[2] SMFI, Department of Mathematics, Physics and Computer Science, University of Parma, viale G.P. Usberti 7/A, 43124 Parma, Italy
[3] Department of Materials Science and Metallurgy, University of Cambridge, 27 Charles Babbage Road, Cambridge CB3 0FS, United Kingdom
[4] Diamond Light Source, Harwell Science and Innovation Campus, Didcot, OX11 0DE, United Kingdom
[5] Escuela Profesional de Ingeniería de Sistemas, Universidad Nacional de Cañete, Jr San Agustín 124, San Vicente de Cañete, Lima, Peru
[6] Laboratorio de Celdas Solares, Universidad Nacional de Barranca, Av. Toribio de Luzuriaga Nro. 376, Mz J, Urbanización La Florida, Distrito y Provincia de Barranca, Peru

E-mail: pjn32@cam.ac.uk

Keywords: magnetisation, micromagnetic simualtions, XMCD-PEEM

Supplementary material for this article is available online

Abstract

The remanent domain structures of composite element magnetic barcodes have been imaged using photo-emission electron microscopy with contrast from x-ray magnetic circular dichroism (XMCD-PEEM) and analysed with reference to the results of micromagnetic simulations. The magnetisation configuration at the end of wide strips is found to be perpendicular to the majority magnetisation direction. This transitions to an incomplete rotation for nominal strip widths below 300 nm and is found to affect the mechanics of magnetisation reversal for nominal strip widths below 200 nm, owing to a difference in magnetisation orientation when an external magnetic field is applied that is just smaller than the magnetic coercivity of the structures and a corresponding change in reversal dynamics. This change in domain structure as strip width decreases is consistent with both the influence of shape anisotropy and with measurements of magnetic hysteresis. The magnetisation reversal characteristics of composite element structures are found to be dependent on the relative magnetisation configurations of neighbouring strips, which in turn are found to vary stochastically upon the application and removal of a magnetic field along the easy axis of the structure. It is found that the application of a canted field is necessary to ensure sharp, consistent magnetisation reversal of bits when writing a binary code. These results confirm that either improved lithography of narrower strips or non-rectangular elements would be necessary to further increase the number of individually programmable bits in a barcode.

1. Introduction

Magnetic barcodes have been identified as versatile, non-volatile magnetic memories that have potential applications in multiplexed molecular identification and biological and chemical assays [1]. The recent development of composite element barcodes (where bits are composed of arrays of narrow magnetic elements) has sought to take advantage of not just the shape anisotropy of individual magnetic strips [2], but also their interaction, via dipolar forces, when elements are brought close together in arrays [3, 4]. The writing of binary digits onto these barcodes is well established [5–9] but refinements to both their design and the writing algorithm are still required in order to fully optimise this process. The reading of information written to these structures is expected to benefit from recent advances in tunnel magnetoresistive sensors that have very high sensitivities [10–12].

Previous efforts were directed towards the maximisation of the number of individually programmable bits —that is, the number of bits to which a code can be written without erasing information carried on other bits. The relationship between magnetic strip width and coercivity was found to have two regions that could be described by power laws, with a crossover between the two regions for widths 150–200 nm [4]. It was hypothesised that the change in power law relation resulted from a change in magnetisation configuration structure and, hence, a change in magnetic reversal mechanism. In order to produce devices that perform predictably and consistently when writing a code, it is necessary to have a good understanding of the magnetisation reversal mechanism: in particular, the effect of the magnetisation structure, both at remanence and with an external magnetic field applied, on their magnetic coercivity and hysteresis.

The magnetisation orientation and domain structure of low aspect ratio permalloy rectangles and squares is well known [13, 14] and it is understood that the magnetostatic coupling of closely spaced permalloy rectangles is strong [15], especially where complete flux closure domains cannot form in the narrow strip limit. This is certainly true in low aspect ratio devices, where magnetisation structures at both ends of an element are found to interact [16], or when the rectangles are closely spaced compared to their width [17]. However, there is a lack of research centring on the remanent magnetisation structure of permalloy rectangles where the aspect ratio, and shape anisotropy, are large enough that the two ends are non-interacting, especially where neighbouring rectangles can interact in an array, and with direct comparison to the structure in wider magnetic strips.

In this work, photoemission electron microscopy employing the x-ray magnetic circular dichroism effect (XMCD-PEEM) is used to directly image the magnetic domain structure of a range of magnetic elements at remanence, after application and removal of a known external magnetic field. The influence of shape anisotropy and dipolar interactions on the remanent state are considered, along with the possible mechanism of the magnetisation reversal process in arrays when an external magnetic field is swept. Our analyses based on micromagnetic simulations are in broad agreement with the imaging data, and overall, our results provide key insights to inform the design of future devices.

2. Methods

The arrays of magnetic structures used in this work are produced by lifting-off a thermally evaporated film that has been patterned by electron beam lithography. Initially, a silicon wafer is prepared by cleaning in solvents and Ti/Au is grown on the surface by thermal evaporation. This Au layer prevents charge build-up during both the electron beam lithography and the XMCD-PEEM measurements—precise lithography and measurement are more critical in these structures than promotion of a large magnetic grain size. 950 PMMA A4 is then spun as a resist to a thickness of ~200 nm and the pattern exposed by electron beam lithography. The sample is developed in MIBK:IPA:MEK 5:15:1 solution. The magnetic layers are grown by thermal evaporation at a base pressure of 1×10^{-7} mbar. First a 5 nm Cr adhesion layer is grown, followed by 15 nm of $Ni_{80}Fe_{20}$ (permalloy), in the absence of an applied magnetic field, and a thin (2 nm) capping layer of Al. This cap is necessary to prevent oxidation of the surface of the film. Lift-off of the pattern is performed in acetone, initially for one hour without agitation, followed by approximately two minutes with ultrasonic agitation. Two samples are measured in this work, one cleaned with one minute of oxygen plasma after lift-off (to remove residue from the lift-off process) and one measured with no further cleaning after lift-off. Both showed quantitatively the same results and so no distinction is made between them in the analysis.

The structures are comprised of a series of magnetic bits, with the nth bit containing n strips each with a width of $w_n = 3200/n$ nm and a space between each strip equal to their width. Figure 1(a) shows a schematic diagram of the architecture for an $n = 3$ bit. All magnetic strips are 15 μm long. Scanning electron microscopy (SEM) images of the arrays of magnetic structures are shown in figures 1(b)–(e). Figure 1(b) shows a complete element of width $w_1 = 3200$ nm, whereas figure 1(c) shows the array with the narrowest elements investigated in this work, with strip width $w_{32} = 100$ nm. Figures 1(d) and (e) then show more magnified images of the tips of these strips. In all these images, we observe a low edge roughness and sharp corners at the tips.

Micromagnetic simulations in this work are performed using Mumax[3], a GPU accelerated program that uses the Landau–Lifshitz formalism [18]. The magnetisation at a given applied external field is estimated using the conjugate gradient method. Typical materials parameters for permalloy were used, with an exchange stiffness of 13 pJ/m and a saturation magnetisation of 860 kA m^{-1} [19]. In simulations, the magnetic elements are 10 μm long, since this reduces computation time whilst not quantitatively affecting the domain structure at the ends of the strips, since they remain unable to interact even at this shorter length. The exception to this is the $n = 1$ strip ($w_1 = 3200$ nm), where the simulated structure is 15 μm long, since the ends can interact, because of the lower aspect ratio and lower shape anisotropy. In these simulations, square cells were used in the plane of the structure, with a cell size between 1 nm × 1 nm (for structures with smaller strip widths) and 4 nm × 4 nm (for structures with larger strip widths).

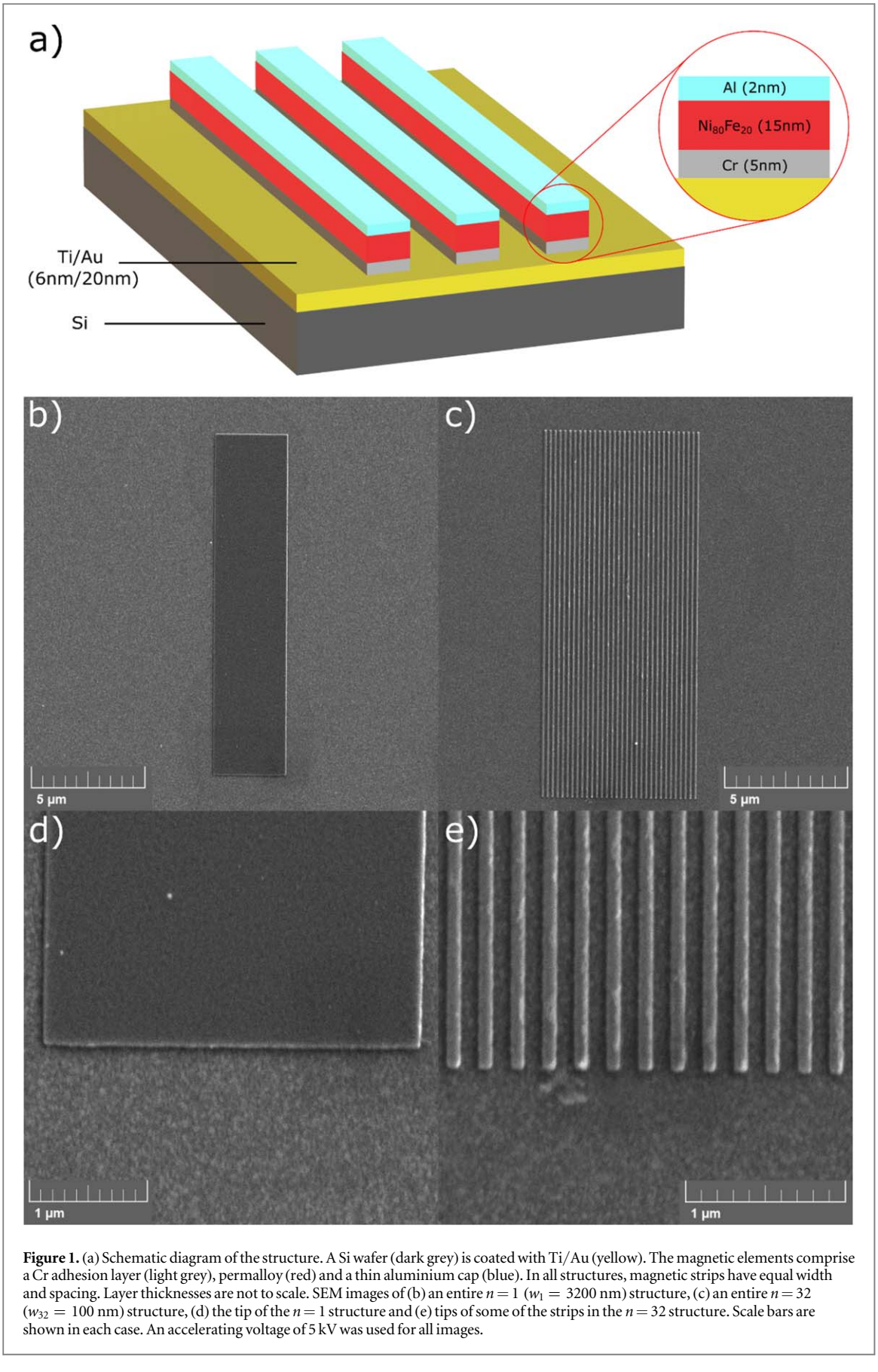

Figure 1. (a) Schematic diagram of the structure. A Si wafer (dark grey) is coated with Ti/Au (yellow). The magnetic elements comprise a Cr adhesion layer (light grey), permalloy (red) and a thin aluminium cap (blue). In all structures, magnetic strips have equal width and spacing. Layer thicknesses are not to scale. SEM images of (b) an entire $n = 1$ ($w_1 = 3200$ nm) structure, (c) an entire $n = 32$ ($w_{32} = 100$ nm) structure, (d) the tip of the $n = 1$ structure and (e) tips of some of the strips in the $n = 32$ structure. Scale bars are shown in each case. An accelerating voltage of 5 kV was used for all images.

XMCD-PEEM is a synchrotron-based technique that exploits x-ray magnetic circular dichroism to obtain elemental selective images of the sample surface, whose contrast is proportional to the magnetization component along the incoming beam direction. Raw PEEM measurements are made both on-and off-resonance of the

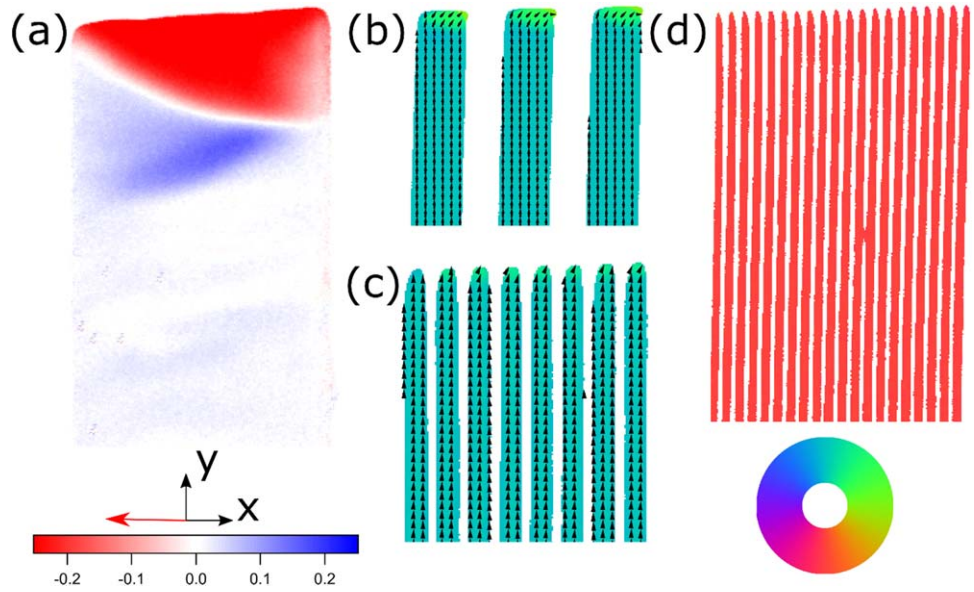

Figure 2. (a) XMCD-PEEM image of a portion of a single strip of width $w_1 = 3200$ nm. The direction of incident x-ray grazing incidence (red arrow) and scale of XMCD asymmetry are shown. The field of view (FOV) for this measurement was 14 μm. (b) Magnetisation vector map of the end of a structure with strip width $w_3 = 1070$ nm. FOV $= 19$ μm. (c) Vector map of the end of a bit with strip width $w_8 = 400$ nm. FOV $= 24$ μm. (d) Vector map of the end of a bit with strip width $w_{20} = 160$ nm. FOV $= 19$ μm. All three vector maps use the same colour wheel, as shown.

magnetic material (here, for Fe, we work at 710.4 eV and 708 eV respectively) to minimise the effect of inhomogeneous illumination of the sample, and with left- and right-hand circularly polarised x-rays. A single XMCD-PEEM scan takes the difference of ten of each of these measurements (40 in total) and the XMCD magnetic image contrast is calculated as the asymmetry of the normalised intensities using,

$$A = (I^R - I^L)/(I^R + I^L)$$

to represent the projection of the local surface magnetisation in the direction of the incident beam. $I^{R/L} = (I^{R/L}_{on} - I^{R/L}_{off})/I^{R/L}_{off}$ are found from the normalised relative intensities of secondary electron emission on and off the L_3 resonance of Fe. The final experimental data are then obtained by averaging many runs of 40 images and therefore improving signal-to-noise and accounting for any small drifts in the system that would blur the data. By obtaining two XMCD asymmetry images, with the sample rotated such that the in-plane projection of the beam lies along two orthogonal directions, a vector map of the in-plane magnetisation can be calculated. XMCD-PEEM measurements in this work were performed on beamline I06 at the Diamond Light Source [20].

3. Results and discussion

3.1. Remanent states of rectangles with varying widths

First, we consider the magnetisation configuration in the $n = 1$ rectangle with width of $w_1 = 3200$ nm. Figure 2(a) shows an XMCD-PEEM measurement of the tip of an $n = 1$ element after application and removal of a strong external magnetic field (50 mT) along the positive y-direction. Here, x-rays are incident close to perpendicular to the magnetic easy axis of the structure. The blue colour corresponds to a magnetisation component parallel to the in-plane beam projection, whereas red corresponds to an antiparallel magnetisation component. At the end of the strip are two adjacent regions with rotation of the magnetisation towards opposite x-directions. These regions are separated by Néel domain walls.

The experimental $n = 3$ ($w_3 = 1070$ nm) magnetisation vector map is shown in figure 2(b), after application and removal of a magnetic field of 50 mT in the positive y-direction. There is clear evidence of magnetisation rotation towards the positive x-direction at the very tip of each strip, with a slight colour change towards a darker blue below the green region at the end of the strip suggesting a very small rotation towards the negative x-direction—this can also be seen with one magnetisation arrow rotating slightly towards the negative x-direction on the leftmost strip.

XMCD-PEEM measurements were also performed on both an $n = 8$ and an $n = 20$ structure ($w_8 = 400$ nm and $w_{20} = 160$ nm). These data are shown in figures 2(c) and (d), with the tips of both structures shown. The $n = 8$ structure was initialised by application and removal of an external field in the positive y-direction, whereas

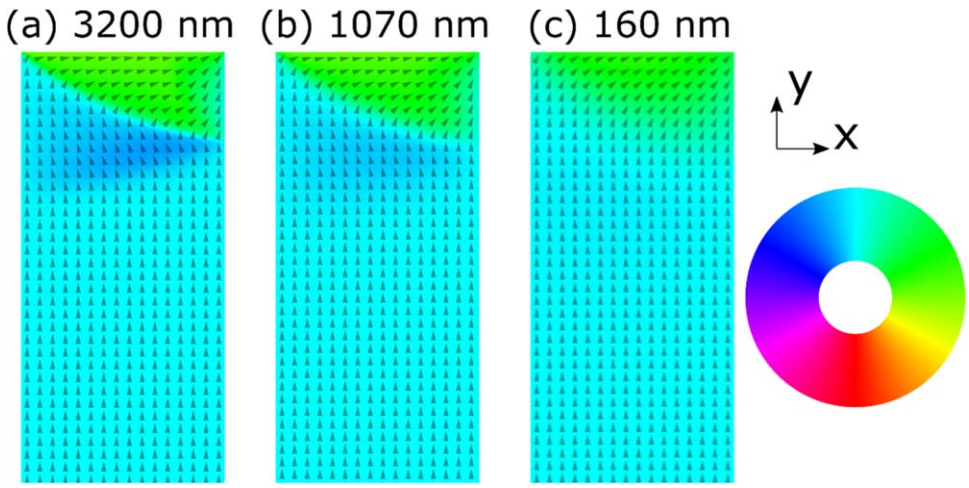

Figure 3. Simulated magnetisation vector maps showing the tips of individual, isolated rectangles with widths (a) $w_1 = 3200$ nm, (b) $w_3 = 1070$ nm, and (c) $w_{20} = 160$ nm. All three vector maps use the same colour wheel, as shown. The images are not shown to the same scale.

the $n = 20$ structure was subjected to a field in the negative y-direction (both of magnitude 50 mT). The main features of the structures are again present, that is, the magnetisation aligns along the easy axis of the structure at remanence and there is a rotation away from this direction at the tips of the strips (in the case of the $n = 20$ device, we see only a small rotation in the top few pixels of the image). We do not see the secondary rotation in a sense opposite to that at the end of the strip in these narrower structures with higher shape anisotropy.

We can look at simulated structures to understand the features at the ends of the strips. Figure 3(a) shows a vector map of the magnetisation of the $w_1 = 3200$ nm rectangle when no external field is applied—the simulation is initialised with uniform magnetisation in the positive y-direction and allowed to relax to remanence. There is clear evidence of rotation of the magnetisation towards both positive and negative x-directions, with the magnetisation at the top of the strip being fully aligned along the positive x-direction.

Figure 3(b) shows the magnetisation vector map of a simulated isolated rectangle of width $w_3 = 1068$ nm at remanence. The structure is exposed to a strong external magnetic field (50 mT) in the positive y-direction, which is then removed. There is a large rotation of the magnetisation at the end of the strip into the positive x-direction and a small rotation towards the negative x-direction below this (much smaller in terms of angle of rotation towards the negative x-direction than that seen in the $w_1 = 3200$ nm structure in figure 3(a)). This simulated result is fully consistent with the experimental result in figure 2(b).

The magnetisation patterns of these structures can be readily compared to one another. As the strips narrow, the enhancement of shape anisotropy makes it energetically unfavourable for the structure seen in figure 2(a) (where there are two regions in the magnetisation configuration that cant in opposite x-directions) to form in the remanent magnetisation when $w_n \lesssim 1000$ nm. We still see one very prominent spin rotation away from the y-direction at the end of the strip—into the positive x-direction. There is evidence for the small rotation in the negative x-direction seen in simulated results of strips with widths less than 1000 nm but these are too small to be resolved in the experimental data. A full perpendicular rotation of the magnetisation is seen at the end of all strips in this limit.

In the case of narrower strips ($w_n \lesssim 300$ nm), we see a change in the remanent magnetisation. Figure 3(c) shows the simulated remanent state of the end of a single 160 nm wide permalloy strip (20 of these strips would comprise an $n = 20$ bit), initialised with magnetisation in the positive y-direction and allowed to relax to remanence. The strip is too narrow and shape anisotropy therefore too significant to allow a full magnetisation rotation into the x-direction to occur—note the direction of the magnetisation arrows at the top of the strip. The change in the nature of the remanent magnetisation configuration between wider strips and this $w_{20} = 160$ nm strip is clear from the simulated results and is even more pronounced as the structures become narrower. These conclusions are consistent with the experimental $n = 20$ vector map in figure 2(d), where only a small magnetisation rotation is visible at the end of each strip (note that the large difference in overall colour between these two images results from magnetising fields being in opposite directions).

Our analysis therefore shows that for decreasing strip width, the configuration of the remanent magnetisation becomes more spatially homogeneous, as expected from increasing shape anisotropy. However, the width ($w_n \approx 300$ nm) at which the magnetisation configuration at the tips of the strips changes between a remanent domain fully perpendicular to the magnetic easy axis and one at an angle to both the easy and hard axis

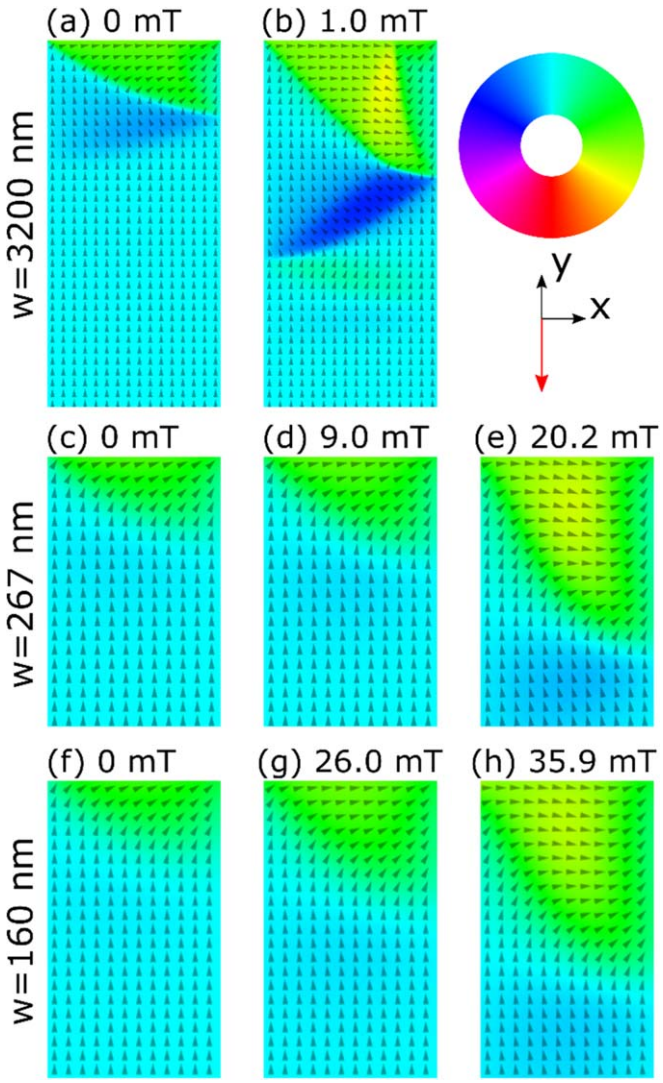

Figure 4. Simulated magnetisation vector maps showing the tips of individual, isolated rectangles when external magnetic fields are applied in the negative y-direction, as shown with the red arrow. A $w_1 = 3200$ nm rectangle with (a) zero field and (b) 1.0 mT applied. A $w_{12} = 267$ nm rectangle with (c) zero field, (d) 9.0 mT and (e) 20.2 mT applied. A $w_{20} = 160$ nm rectangle with (f) zero field, (g) 26.0 mT and (h) 35.9 mT applied. All vector maps use the same colour wheel, as shown. (a) and (f) are reproduced from figure 3 (with differently sized arrows) for ease of comparison. The images are not shown to the same scale.

in these simulations does not coincide with the strip width ($w_n \approx 200$ nm) at which we found a change in power law relationship in measurements of magnetic hysteresis [4].

3.2. The reversal process of isolated rectangular magnetic elements

We now explore magnetisation reversal in our arrays of magnetic structures, thus addressing magnetisation configurations in varying applied fields. In all the simulations shown in figure 4, the structures were initially magnetised with a strong applied field (50 mT) in the positive y-direction. The results shown are the magnetisation configurations with a field applied along the negative y-direction (as shown with the red arrow). We initially consider a strip with width $w_1 = 3200$ nm. Figure 4(b) shows the magnetisation configuration when a magnetic field of 1 mT is applied—this is just below the coercive field of ~1.2 mT. Comparison with the remanent domain structure in figure 4(a) (reproduced from figure 3(a)) shows that the region with magnetisation rotated away from the positive y-direction has stretched down the strip. Notable is the rotation of spin states in the green region in the remanent state towards the negative y-direction—the spin-states in the yellow region have rotated away from pointing slightly upwards in the remanent state to now pointing downwards after application of this external field. In this wide strip limit, the magnetisation reversal is mediated by a zigzag domain structure [21, 22], with reverse domains nucleating throughout the zigzag. The dynamics of this reversal after increasing the applied field from 1 mT to 1.5 mT are shown in figure S2 in the supplementary material (available online at stacks.iop.org/MRX/8/096103/mmedia). Further simulations (not shown)

demonstrate that a full zigzag would not be seen for $n = 2$ and above, owing to the stronger shape anisotropy in these narrow structures.

When applying the same process to narrower strips, we see some different behaviours. Figures 4(c)–(e) show simulations of the magnetisation at the end of a single rectangle of width $w_{12} = 267$ nm when magnetic fields of 0 mT, 9 mT and 20 mT are applied in the negative y-direction, respectively. The remanent magnetisation at the tip of the strip is canted with respect to the x- and y-axes. In figure 4(d), we find that the magnetisation rotates parallel to the x-direction at the tip of the strip at an applied magnetic field (9mT) that is much smaller than its coercivity (20.3 mT). Figure 4(e) shows the magnetisation configuration at 20.2 mT—note the presence of a yellow region in the magnetisation, indicating spins that point at an angle to both the positive x-direction and negative y-direction. A further increase of the magnetic field to 20.3 mT causes further rotation of spins in this yellow region. The yellow region then expands down the strip and magnetisation reversal is initialised. The domain wall propagation along the strip and reversal of its majority magnetisation gives the familiar Barkhausen jump in the magnetisation [23, 24]. The dynamics of this reversal are shown in figure S4 in the supplementary material. The results here are consistent with previous Lorentz microscopy [22, 25] and magnetic force microscopy [26] imaging performed on individual permalloy rectangles.

We therefore find that the magnetisation reversal of this rectangle of width $w_{12} = 267$ nm is by the same mechanism as for the $w_3 = 1070$ nm rectangle (see figure S3 in the supplementary material). Note also that the rotations of spin-states into opposite x-directions in the magnetisation structures at the ends of these strips reappear upon application of an external field along the y-direction opposite to the majority magnetisation of the bit [27]; their absence in the remanent state has no specific impact on their magnetic reversal characteristics.

We see a different behaviour in structures of width $w_n \lesssim 200$ nm. Figures 4(f)–(h) show the magnetisation configuration in a simulation of a strip with width $w_{20} = 160$ nm. From the remanent state (figure 4(f)), we apply an external magnetic field in the negative y-direction and find a quantitatively different magnetisation configuration from the wider strips explored above. Figures 4(g) and (h) show the top of this rectangle when fields of 26.0 mT (when the magnetisation at the tip of the strip first aligns along the x-axis) and 35.9 mT (just less than the coercive field of ~36.0 mT) are applied, respectively. Notice the direction of magnetisation at the top left of figure 4(h)—particularly the top two arrows on the left-hand side. In figure 4(h), the structure cants more towards the x-direction than seen in the wider rectangles (see figure 4(e)). As a result, the point on the strip where magnetisation reversal is instigated is different—in this case, increasing the applied field to 36.0 mT initialises reversal from this top left point, without the need for a structure in the centre of the strip (like the yellow region in figure 4(e)) to stretch down the strip first. The dynamics of this reversal are shown in figure S5 in the supplementary material.

We postulate that this change in magnetisation configuration of isolated permalloy rectangles, when an external field is applied antiparallel to the majority magnetisation close to remanence and the corresponding change in reversal dynamics, is the reason for a change in power law relationship between coercivity and strip width for widths $w_n \lesssim 200$ nm found in our previous work [4]. The increase in shape anisotropy for narrower strips therefore fundamentally changes the magnetisation reversal mechanism, with reversal able to instigate for more spatially homogeneous magnetisation configurations than for wider strips, where reversal must be instigated by the propagation down the strip of a region of magnetisation from the middle of the tip.

3.3. The reversal process of arrays and the influence of remanent magnetisation orientation

We now investigate the role of the remanent magnetisation configurations (Section A) on the magnetisation reversal process of a composite element structure. In the simulated hysteresis loop of figure 5(a) we have considered an $n = 20$ structure ($w_{20} = 160$ nm) that was initialised with a random configuration of magnetisation before application and removal of a 40 mT along the negative y-direction. The hysteresis is quite broad on the reversal when applying a magnetic field in the positive y-direction. By analysing the magnetisation pattern after each 1 mT step, we can understand the overall reversal mechanism. The leftmost strip reversed its magnetisation at 33 mT and initialised a cascade, with neighbouring strips also switching in sequence, but this stopped, owing to the presence of anti-aligned magnetisation along the x-direction at the tips of the strips. Figure 5(b) shows the stable magnetisation state at 33 mT on the side of the structure where the cascade originated—the left-hand strips have undergone magnetisation reversal and appear blue instead of red in this vector map. The seventh strip, counting from the left, has not reversed, despite also having magnetisation pointing to the right at its tip—the local field caused by a negative x-aligned magnetisation on the eighth strip meaning it needs a greater external field to reverse its magnetisation. Figure 5(e) shows the magnetisation after application of 34 mT. The increase in external field has allowed two more strips to reverse their magnetisation, but again, a full cascade of magnetisation reversal is prevented by the misalignment of the transverse domains at the ends of the strips. Increasing the field yet further allows more strips to reverse their magnetisation. A 36 mT field has been applied to the array shown in figure 3(d). The field is sufficiently large now that cascades can begin

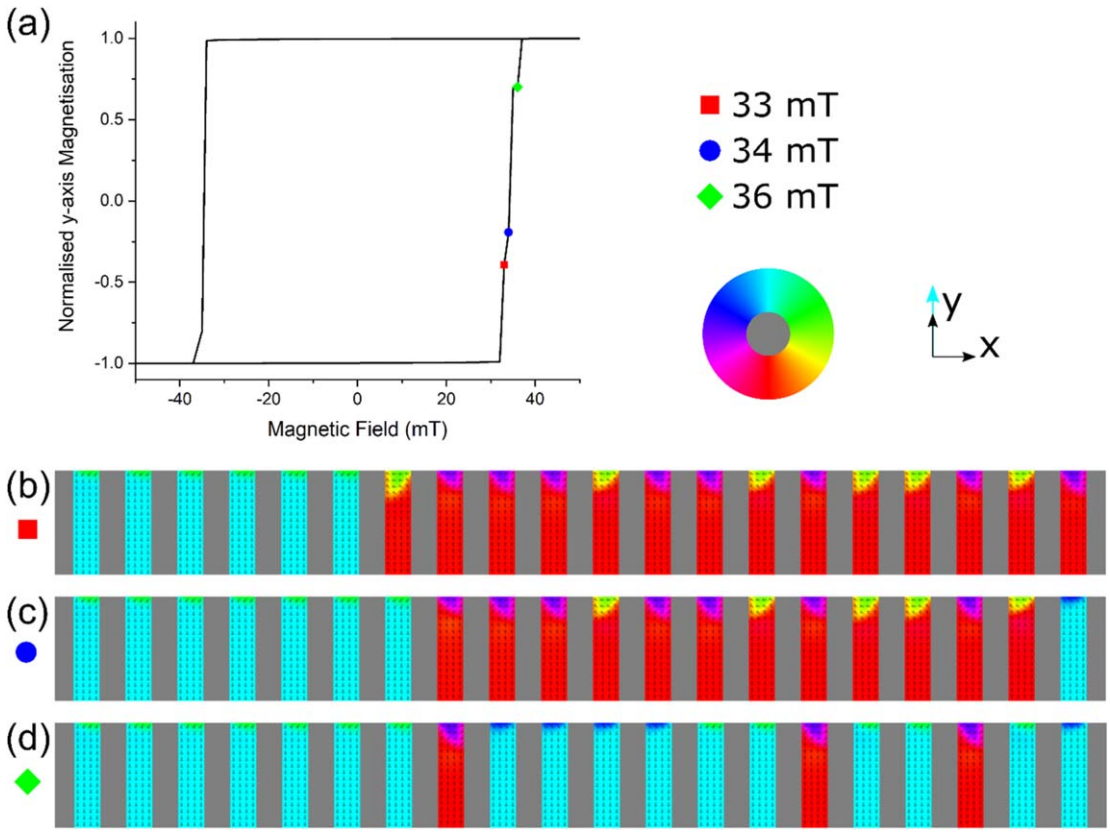

Figure 5. (a) Simulated hysteresis (normalised magnetisation along the easy axis) of an $n = 20$ ($w_{20} = 160$ nm) bit initialised with a random magnetisation configuration at the ends of the strips. The points marked in red, blue and green correspond to the vector maps shown. Simulated magnetisation configuration of the top of this bit after initial magnetisation of the structure with a field with a magnitude of 50 mT in the negative y-direction and application of an external magnetic field of magnitude (b) 33 mT, (c) 34 mT and (d) 36 mT in the positive y-direction, as shown with the light blue arrow. The colour wheel for the vector maps is shown.

in strips that are more central in the array. We again see some strips where transverse domains align such as to effectively pin their magnetisation in the negative y-direction. This effect of transverse domains at the ends of the strips pointing in different directions is a separate issue from edge roughness, which is also expected to induce steps in the hysteresis [28].

These results have clear implications for writing to barcodes with many bits with closely spaced coercivities. As discussed in our previous work, a precisely programmed field sweep in positive and negative directions along the magnetic easy axis is required to reliably write binary digits [3, 4]. A concern, therefore, is that a bit may not become fully magnetised if a field is applied that is only sufficient to initialise cascades of outer strips but not to fully reverse the magnetisation of the element. Were the binary code to be measured, there would therefore be a reduction in signal in readout and a potential loss of information. It is important, then, to consider the domain structure seen in real devices to see what impact this might have on their operation.

It is instructive to look at the magnetisation configuration structure of a real magnetic array at remanence after magnetic field sweeps of 50 mT-a magnitude that would be encountered when writing binary digits onto a barcode device but is much larger than the coercivity of the wider strips in the device. Here, the exact state that the structure enters upon magnetic reversal appears to be somewhat stochastic. Consider the experimental data in figures 6(a)–(c): the $n = 3$ structure enters a range of remanent states after exposure to a strong external field (a magnetic field of at least 50 mT is applied and removed in both the positive and negative y-directions and the structure is allowed to relax to the remanent state). Many remanent states the ends of the strips align in the x-direction but some are found to anti-align.

Consider also the ideal case represented by simulations, here performed to look at the domain structure of an $n = 4$ bit ($w_4 = 800$ nm) throughout its hysteresis in figures 6(d)–(f). The structure was initialised with a uniform magnetisation along the green arrow and the energy minimised to give the remanent state shown in figure 4(d), where the magnetisation at the tips of the strips is aligned in the positive x-direction. A strong field (50 mT) was applied in the negative y-direction, as shown (figure 6(e)) and reduced back to zero, leaving the structures at remanence again. The resulting remanent state is seen in figure 6(f). Here it can be seen that one small transverse domain has become anti-aligned with the rest without any final change in the majority

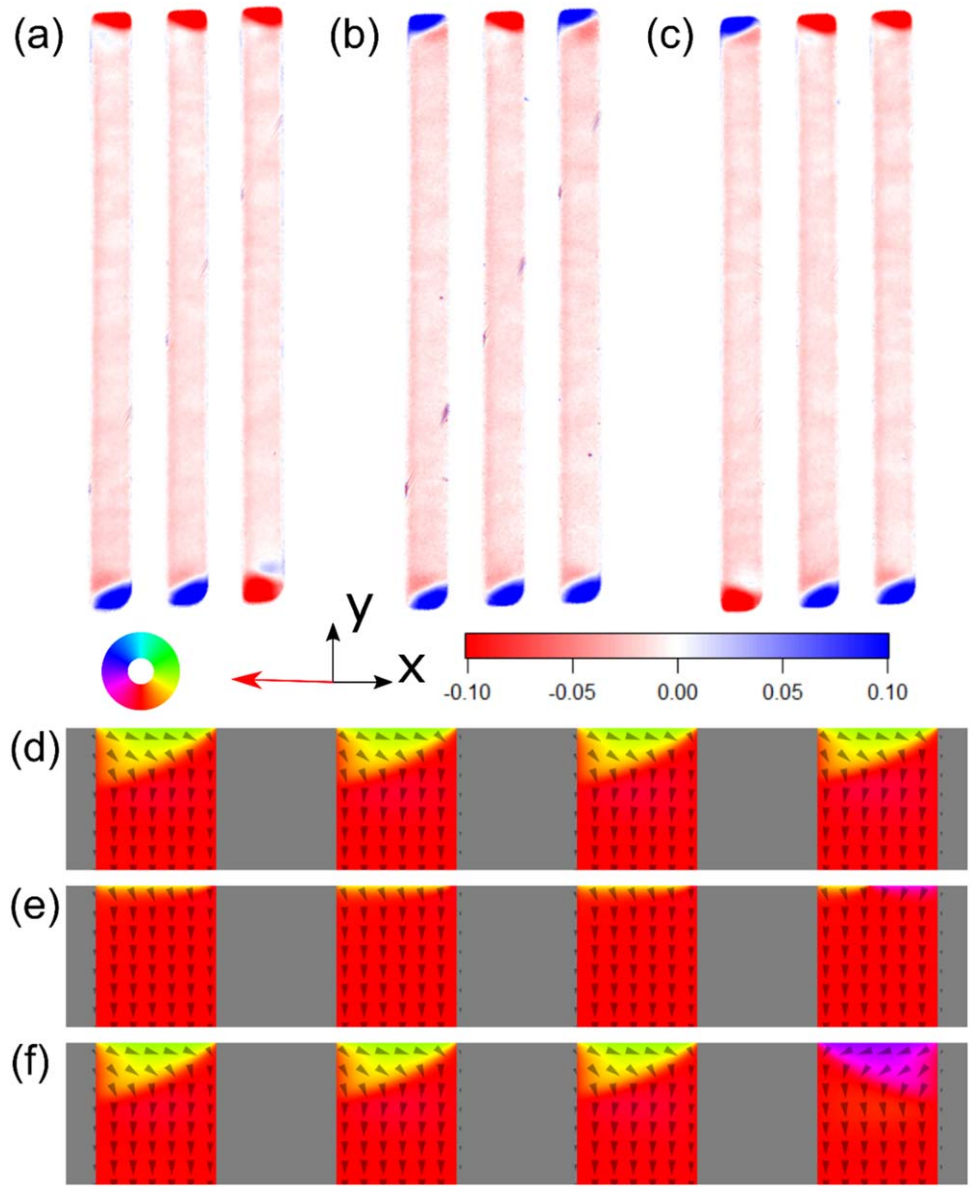

Figure 6. (a)–(c) XMCD-PEEM measurements on an $n = 3$ ($w_3 = 1070$ nm) bit, each measured after application and removal of consecutive strong fields (50 mT) in the positive and negative y-direction. The in-plane projection of x-ray grazing incidence is shown with the red arrow, as is the scale of the XMCD asymmetry. FOV $= 24\ \mu$m. Small lines seen cutting across the images are artifacts from the PEEM imaging, owing to the configuration of the PEEM setup. (d)–(f) The magnetisation configurations of a simulated $n = 4$ ($w_4 = 800$ nm) bit, d) initialised in a state where all magnetisation states at the end of the strip align in the positive x-direction and no external field applied, (e) in an applied 50 mT external field in the negative y-direction, and (f) after the removal of the external magnetic field. The colour wheel for the simulated vector maps is shown.

magnetisation direction of any of the elements. This is a behaviour that is dependent on the exact magnitude of the applied external magnetic field but occurs consistently at these values.

This is a direct consequence of the dipolar interactions between strips and the different environments experienced by strips at the edge of the array. As the magnetic field is increased, the area with magnetisation rotation into the x-direction effectively compresses as its moments rotate towards the field—the majority magnetisation direction of the strip. When the field is sufficiently large, the top domain in the right strip splits in two (see the top of the rightmost strip in figure 6(e)), with a region with a magnetisation component in the negative x-direction growing from the right. This mirrors the lowest energy, maximally symmetric solution in the high field regime. (A further increase in field would allow the same structure to form in the other strips.) When the field is removed, dipolar interactions encourage magnetisation towards the negative y-direction to endure at the left-hand side of this strip, allowing the domain pointing towards the negative x-direction to grow from the right. The result at remanence is therefore a flipping of the magnetisation in the x-direction at the tip of the strip. The central and left strips relax into their initial configuration. This pattern is mirrored in the domains at the bottom of the strips (not shown).

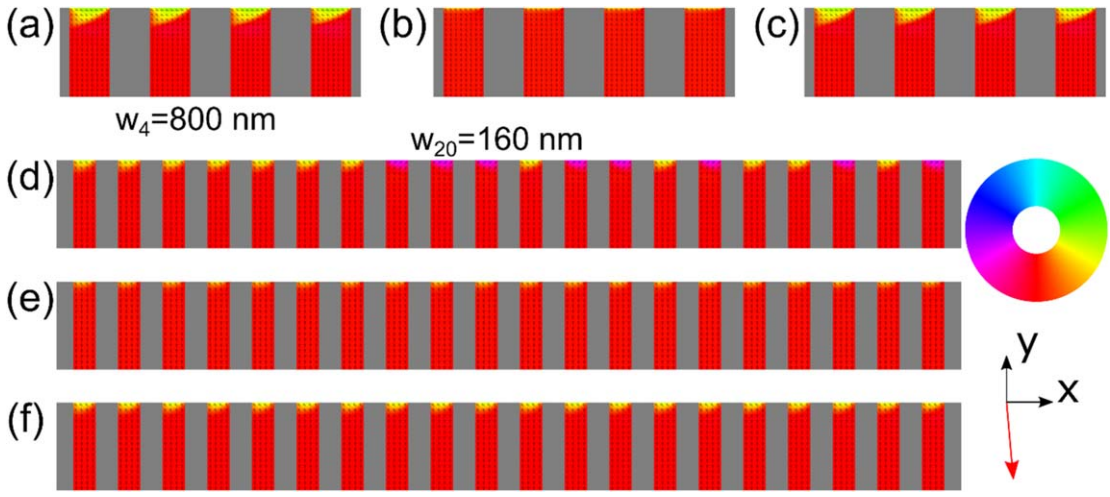

Figure 7. Simulated magnetisation configurations of the tops of magnetic elements. An $n = 4$ ($w_4 = 800$ nm) bit a) at remanence as in figures 6(d), (b)) after application of a 50 mT external magnetic field at a 5° angle to the *y*-axis (red arrow), and (c) after removing the field and returning to remanence. An $n = 20$ ($w_{20} = 160$ nm) bit (d) initialised at remanence with majority magnetisation in the negative y-direction but random x-canting of transverse domains, (e) after application of a 60 mT external magnetic field at a 5° angle to the *y*-axis (red arrow), and (f) after removing the field and returning to remanence. The colour wheel for the simulated vector maps is shown.

Therefore, even in the ideal case presented by our simulations, magnetisations at the ends of the strips naturally misalign in opposite x-directions when treated simply with a field along the easy axis of the structure. Whilst it is true that small field applications will not cause misalignment, the application of relatively strong magnetic fields (of the order of 50 mT), in both positive and negative y-directions, when writing a code to bits with the narrowest strips, is likely to result in some misalignment in bits with wider strips. Such field sweeps are necessary for the writing of binary digits. The inhomogeneity of real devices will also add an element of randomness to the final structure, giving us the stochastic behaviour observed in our XMCD-PEEM measurements.

The lack of natural alignment of magnetisation at the ends of strips has implications for the writing of codes to these devices. We have shown that magnetisation reversal initiates at the outer strips in a bit, which then changes the local effective field and triggers neighbouring strips to also begin reversal. However, we find by simulation that anti-alignment can hinder this reversal cascade through the bit and give steps in the hysteresis. A possible solution, therefore, is to apply the initialising field (that puts all bits into the '0' state before programming) at an angle to the magnetic easy axis to promote full alignment of the small transverse domains in each strip. This canting of the magnetic field also needs to be applied throughout writing of the code to maintain this transverse domain alignment. Our simulations suggest that application at an angle of only 5° would be sufficient to keep all strips aligned in the $n = 4$ bit. This is shown in figures 7(a)–(c), where we recreate the simulation shown in figures 6(d)–(f) but with the applied field at an angle of 5° towards the x-direction, as shown with the red arrow. We have also simulated the effect of a canted field on the structure simulated in figure 5. In this case, the random orientation of the transverse domains at the ends of the strips can be corrected into a state with transverse domains all pointing towards the positive x-direction, as shown in figure 7(d). This can be achieved with an initialising field of 60 mT, again at 5° to the *y*-axis, as shown with the red arrow. Performing sweeps of external magnetic field to obtain the hysteresis loop demonstrates that all strips reverse at the same applied field. It is possible that the angle of magnetic field application might need to be larger in real devices, because of the effects of edge roughness and inhomogeneity in the arrays of magnetic structures, and to take account of the chaotic behaviour seen in some of the reversal dynamics explored in the supplementary material.

4. Conclusions

The results of XMCD-PEEM measurements and micromagnetic simulations of composite element magnetic barcodes have informed both their design and the algorithm needed to consistently write codes to them. The existence of a change in magnetisation configuration in these structures close to remanence when strip width is less than 200 nm is unavoidable in devices comprised entirely of composite element, rectangular bits. To increase the number of individually programmable bits in a barcode device, therefore, bits must be developed with narrower strip widths, or investigations must be made into elements with shapes that may be magnetically

harder than a rectangle. The alignment of remanent, transverse domains in the strips of individual bits is critical to ensure consistent magnetic performance; this can be promoted by using a magnetising field that is canted with respect to the easy axis of the bit when both initialising the state prior to writing a code and during the code writing process itself.

Acknowledgments

This work was carried out initially with the financial support of the Universidad Nacional de Barranca (UNAB) and completed with the help of the Universidad Nacional de Cañete (UNDC). The grant was approved by the '*Congreso de la República de Perú, Ley* Nro 30879–2019 (*Disposiciones complementarias Octogésima segunda*)'. In particular, we would like to thank C.E. Villanueva Aguilar and J.H. Jhoncon Kooyip from UNDC and L.E. Carrillo Diaz from UNAB for their help and encouragement throughout this work. The authors are grateful for the assistance of Dr C.L. Truscott in obtaining the SEM images shown in figure 1. This work was carried out with the support of Diamond Light Source, instrument I06 (proposal MM24373).

Data availability statement

The data that support the findings of this study will be openly available following an embargo at the following URL/DOI: https://doi.org/10.17863/CAM.72077. Data will be available from 13 September 2021.

ORCID iDs

P J Newton https://orcid.org/0000-0002-4581-8581
N B Devlin https://orcid.org/0000-0002-3133-0235
M Ghidini https://orcid.org/0000-0002-1905-2455
D Backes https://orcid.org/0000-0002-1019-3323
F Maccherozzi https://orcid.org/0000-0003-4074-2319
C H W Barnes https://orcid.org/0000-0001-7337-7245

References

[1] Llandro J, Palreyman J J, Ionsecu A and Barnes C H W 2010 *Med. Biol. Eng. Comput.* **48** 977
[2] Adeyeye A O, Bland J A C, Daboo C, Lee J, Ebels U and Ahmed H 1996 *J. Appl. Phys.* **79** 6120
[3] Love D M, Vyas K N, Fernandez-Pacheco A, Llandro J, Palfreyman J J, Mitrelias T and Barnes C H W 2015 *RSC Adv.* **5** 10211
[4] Newton P J, De Los Santos Valladares L, Celis Rojas R and Barnes C H W 2019 *Appl. Phys. Lett.* **115** 162404
[5] Jeong J R, Llandro J, Hong B, Hayward T J, Mitrelias T, Kopper K P, Trypiniotis T, Steinmuller S J, Simpson G K and Bland J A C 2008 *Lab Chip* **8** 1883–7
[6] Hong B, Hayward T J, Jeong J R, Cooper J F K, Palfreyman J J, Mitrelias T, Ionescu A, Bland J A C and Barnes C H W 2009 *J. Appl. Phys.* **105** 034701
[7] Mitrelias T, Cooper J F K, Vyas K N, Palreyman J J, Hong B, Hayward T J and Barnes C H W 2010 *J. Appl. Phys.* **107** 09B319
[8] Hayward T J *et al* 2010 *J. Phys. D: Appl. Phys.* **43** 175001
[9] Palfreyman J J, Beldon P, Hong B, Vyas K N, Cooper J F K, Mitrelias T and Barnes C H W 2010 *AIP Conference Proceedings* **1311** 184
[10] Jin Z, Oogane M, Fujiwara K and Ando Y 2017 *J. Appl. Phys.* **122** 174502
[11] Abrunhosa S, Merazzo K J, Costa T, Sandig O, Franco F and Cardoso S 2020 *Sens. Actuators, A* **303** 111673
[12] Khan M A, Sun J, Li B, Przybysz A and Kosel J 2021 *Engineering Research Express* **3** 022005
[13] Gomez R D, Luu T V, Pak A O, Kirk K J and Chapman J N 1999 *J. Appl. Phys.* **85** 6163
[14] Barthelmess M, Pels C, Thieme A and Meier G 2004 *J. Appl. Phys.* **95** 5641
[15] Hankemeier S, Frömter R, Mikuszeit N, Stickler D, Stillrich H, Pütter S, Vedmedenko E Y and Oepen H P 2009 *Phys. Rev. Lett.* **103** 147204
[16] Jelli J, Lebecki K M, Hankemeier S, Fromter R, Oepen H P and Nowak U 2013 *IEEE Trans. Magn.* **49** 1077–81
[17] Krasyuk A, Nepijko S, Oelsner A, Schneider C M, Elmers H J and Schönhense G 2007 *Appl. Phys. A* **88** 793–6
[18] Vansteenkiste A, Leliaert J, Dvornik M, Helsen M, Garcia-Sanchez F and Van Waeyenberge B 2014 *AIP Adv.* **4** 107133
[19] Shull R D, Kabanov Y P, Gornakov V S, Chen P J and Nikitenko V I 2016 *J. Magn. Magn. Mater.* **400** 191–9
[20] Dhesi S S *et al* 2010 *AIP Conf. Proc.* **1234** 311
[21] Chumakov D, McCord J, Schäfer R, Schultz L, Vinzelberg H, Kaltofen R and Mönch I 2005 *Physical Review B* **71** 014410
[22] McVitie S and Chapman J N 1997 *Microsc. Microanal.* **3** 146–53
[23] Smyth J F, Schultz S, Fredkin D R, Kern D P, Rishton S A, Schmid H J, Cali M and Koehler T R 1991 *J. Appl. Phys.* **69** 5262
[24] Vazquez M and Chen D- 1995 *IEEE Trans. Magn.* **31** 1229–38
[25] Hefferman S J, Chapman J N and McVitie S 1991 *J. Magn. Magn. Mater.* **95** 76–84
[26] Koo H, Luu T V and Gomez R D 2000 *J. Appl. Phys.* **87** 5114
[27] Yuan S W, Bertram H N, Smyth J F and Schultz S 1992 *IEEE Trans. Magn.* **28** 3171–3
[28] Deak J G and Koch R H 2000 *J. Magn. Magn. Mater.* **213** 25–31